Materials and Design 161 (2019) 95–105

Contents lists available at ScienceDirect

Materials and Design

journal homepage: www.elsevier.com/locate/matdes

Over five-times improved elongation-to-fracture of dual-phase 1180 steel by continuous-bending-under-tension

Camille M. Poulin, Yannis P. Korkolis, Brad L. Kinsey, Marko Knezevic *

Department of Mechanical Engineering, University of New Hampshire, Durham, NH 03824, USA

HIGHLIGHTS

- Elongation-to-fracture of DP 1180 steel under continuous-bending-under-tension is investigated.
- Over five-times improved elongation of DP 1180 is achieved by continuous-bending-under-tension relative to simple tension.
- Continuous-bending-under-tension facilitates uniform depletion of ductility preventing a localized flow followed by necking.
- Strength of the material can be significantly improved by continuous-bending-under-tension processing.

GRAPHICAL ABSTRACT

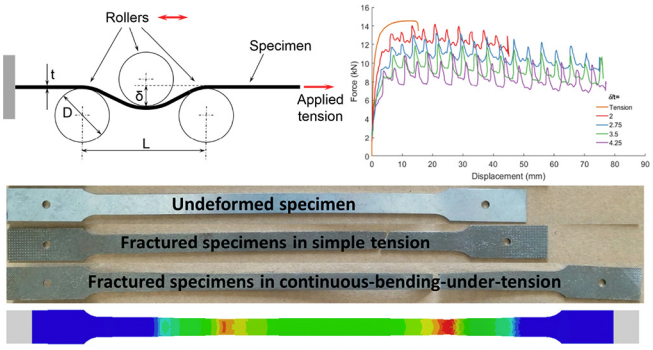

ARTICLE INFO

Article history:
Received 14 September 2018
Received in revised form 27 October 2018
Accepted 8 November 2018
Available online 09 November 2018

Keywords:
Elongation
Plasticity
Fracture
Advanced high strength steels
Continuous-bending-under-tension

ABSTRACT

This paper reports the main results from an experimental investigation into the improved elongation-to-fracture (ETF) of the advanced high strength steel (AHSS) dual-phase (DP) 1180 by subjecting the material to the continuous-bending-under-tension (CBT) process. The investigation is carried out using a recently developed testing apparatus, where the specimen flows in a reciprocating fashion through a set of three rollers while it is continuously pulled in tension. The process parameters such as the roller depth defining the amount of bending and wrapping around the rollers and crosshead velocity applying the tensile force to the specimen are varied to maximize the ETF of the material. From the recorded force vs. displacement curves along the rolling direction (RD), 45°, and transverse direction (TD), ETF of DP 1180 is found to improve with the crosshead velocity and with the bending depth up to a certain level, after which it decreases. The optimal parameters of 1.35 mm/s for the crosshead velocity and 3.5 for the normalized bending depth improve ETF of the material over five times in every testing direction relative to simple tension tests. The role of CBT in preserving high integrity of the material to large plastic strains is discussed.

1. Introduction

In order to achieve lighter, higher performing, and more crashworthy vehicle structures, advanced high strength steels (AHSS) are being developed and incorporated into designs. Premier examples of AHSS are dual-phase (DP) steels. Understanding and optimizing of the microstructure of DP steels in order to achieve higher strength, work hardening rate and formability, along with higher energy absorption during crash loading conditions is ongoing research [1–5]. These properties are primarily governed by the volume fraction and spatial distribution of martensite and ferrite phases with contrasting mechanical characteristics, as well as grain size and crystal lattice orientation distributions

* Corresponding author at: University of New Hampshire, Department of Mechanical Engineering, 33 Academic Way, Kingsbury Hall, W119, Durham, NH 03824, USA.
E-mail address: marko.knezevic@unh.edu (M. Knezevic).

https://doi.org/10.1016/j.matdes.2018.11.022

per phase. It has been shown that simultaneous improvement of strength and ductility in DP steels is possible by distributing the phases [6,7]. The deformation of DP steels is highly heterogeneous, and, therefore, the overall behavior of DP steels critically depends on the evolution of the local mechanical fields among the phases. For example, large ferrite grains suitably oriented for crystallographic slip can deform plastically earlier than small ferrite grains [8]. Severe strain localization followed by void initiation have been observed within large ferrite grains, ferrite channels between bulky martensite regions, and at martensite–ferrite phase interfaces [2,8,9]. As a result, these materials can exhibit limited ductility prior to fracture (often <10–15%) during sheet metal forming operations [10–15]. Additionally, these materials require high forming forces due to their high strength. There is, therefore, a permanent interest to further optimize their microstructure aiming at higher ductility and energy absorption during crash loading conditions on one hand and at lower energy consumption in their metal forming operations on the other [16]. The latter fuels the research in conceiving innovative sheet metal forming processes. In particular, the accent is on discovering processes that exploit the intrinsic ductility of the material throughout the sheet, circumventing localized necking and the early failure that this triggers. One such process is continuous-bending-under-tension (CBT), which achieves strain levels well above those generally observed in conventional forming limited by necking [17–19].

The beneficial effect of superimposing bending on tension to enhance the elongation-to-fracture (ETF) of metal sheets was recognized in [20], as well as in sheet forming involving drawbeads [21]. During CBT processing, the material in the gauge length of the specimen is continuously bent and unbent by three rollers. Fig. 1 shows a schematic of the process and a photograph of the CBT apparatus at the University of New Hampshire [17]. The rollers induce bending-under-tension to the region of the specimen they are currently engaging. The process could facilitate the material in the form of a strip or a sheet to deform with a lower force, as the deformation is primarily achieved through the bending process. Moreover, localization of the deformation can be delayed through the CBT processing, thus the material can incrementally elongate beyond what can be achieved during standard simple tension (ST). For example, the percent elongation at fracture for an AISI 1006 steel increased from 22% to 290% [18]. Past research for AA6022-T4 has shown that the concentrated deformation in the fracture location upon simple tension is similar to the deformation over the entire gauge length of a CBT processed specimen [17].

There are other sheet metal forming processes that produce local deformation, similar to the 3-point bending effects in CBT. For example, in spin forming, a stationary tool contacts a spinning blank to create an axisymmetric component [22–24]. Alternatively, in incremental sheet forming (ISF) a hemispherical tool locally deforms the sheet. In both processes, only a small portion of the sheet is plastically deformed at each instant. Similar to the CBT process, the strains achieved during spin forming and ISF are well above what is possible in standard sheet forming. The CBT process essentially delays the localization and necking, and as a result, facilitates a more uniform depletion of ductility throughout the sheet as opposed to necking, where the majority of the sheet (i.e., outside of the necked region) has ample remaining ductility [25–28]. If the CBT process is interrupted after a certain number of cycles, any residual ductility as well as strength of the material can be assessed by secondary tensile tests [17].

In this paper, CBT processing of DP 1180 is investigated through a parametric study using a recently built experimental apparatus [17]. To this end, the parameter space for CBT processing is explored by

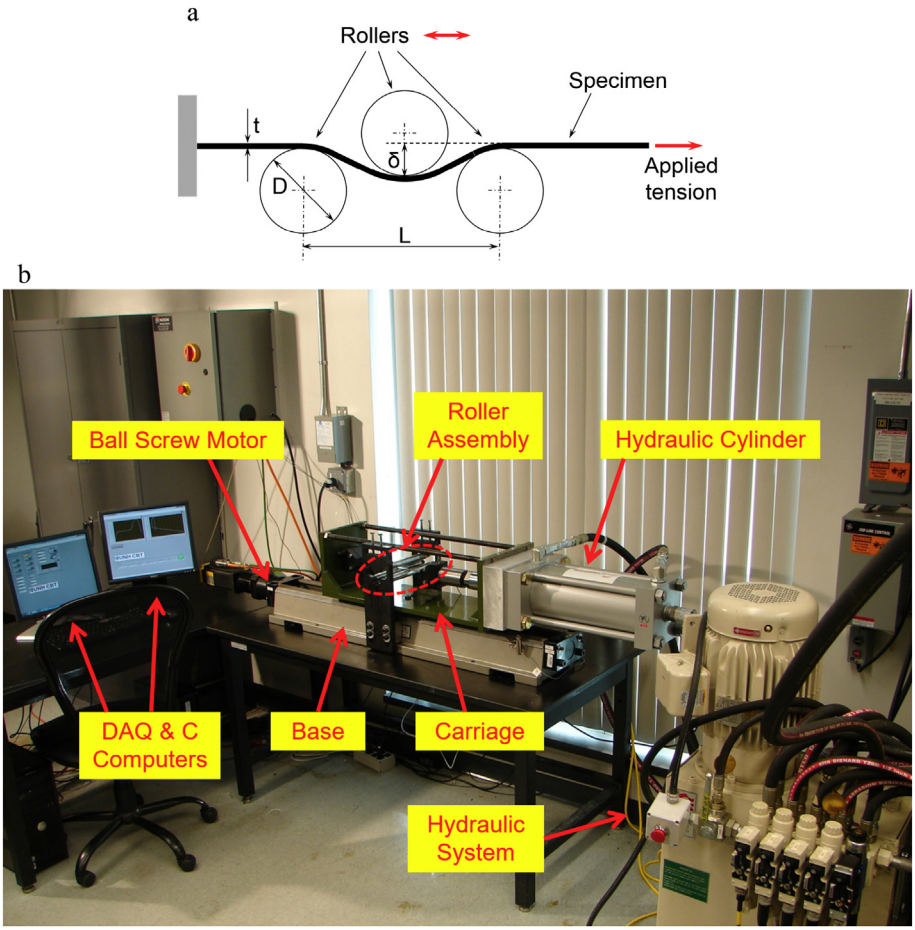

Fig. 1. (a) Schematic of the continuous-bending-under-tension (CBT) test/process. (b) A photograph of the CBT apparatus at UNH with the main components identified.

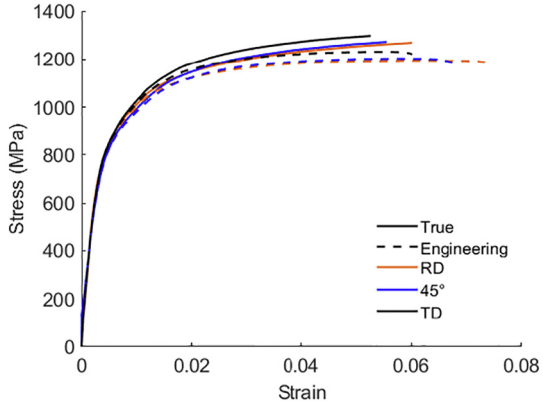

Fig. 2. Engineering stress-strain (dashed line) and true stress-strain (solid lines) curves for DP 1180 along the rolling direction (RD), 45°, and transverse direction (TD) recorded in simple tension under a strain rate of 0.001/s.

varying the normalized bending depth and crosshead velocity, i.e., the velocity of the applied tension in Fig. 1a, the two main parameters in CBT processing. Force vs. displacement curves as a function of the parameters are presented and described. The material is also characterized through uniaxial tension tests, which is used as a reference for assessing the behavior in CBT. The tests are performed at three angles with respect to the rolling direction (RD) to evaluate the anisotropy. To better understand the kinematics of the process and the development of local stress and strain fields a finite element (FE) simulation of CBT is carried out. Finally, the behavior of DP 1180 sheets upon CBT processing to a certain number of CBT cycles is investigated. Results and insights for these investigations are presented are discussed in this paper.

2. Material and experiments

The DP steel investigated in this study is a commercial DP 1180 steel sheet from US Steel's continuous annealing line [29]. This is an auto-body material and, as such, can benefit from the enhancement in its ETF. We begin by describing the behavior of the material in ST, including its strain rate-dependence. Specimens were machined from a 1.04 mm thick DP 1180 sheet with respect to 0° (rolling direction, RD), 45°, and 90° (transverse direction, TD) to the rolling direction of the sheet material. Fig. 2 shows the ST test results for both engineering and true stress-true strain data. While the material has been characterized to exhibit some elastic anisotropy [30], the material shows a small amount of plastic anisotropy in the plane of the sheet in terms of the flow stresses. As is evident, the material exhibits high strength and high stiffness but the uniform ductility of the material is rather small with engineering strain values <8% at fracture. Some limited dependence with orientation is measured for ETF. The plastic deformation in ST is limited by shear localization accompanied with necking followed by fracture, which will be depicted later. The narrow localization region experiences very large plastic strain, while the remainder of a fractured specimen has a substantial amount of remaining ductility, which is never exploited due to the localization [31]. In contrast to ST, the CBT process is set forth to exploit ductility of the entire specimen.

Due to varying rates of the material deformation during CBT processing, the strain-rate sensitivity of the material is essential to assess. Thus jump tests, i.e., tension tests where the strain-rate is varied during the test, were conducted [31]. Four strain-rates of 0.0001, 0.001, 0.005, and 0.01/s were used. Fig. 3 shows the results from the jump test. Based on the data obtained, the strain-rate sensitivity of the material can be calculated using $m = \frac{\ln\frac{\sigma_2}{\sigma_1}}{\ln\frac{\dot{\varepsilon}_2}{\dot{\varepsilon}_1}}$, where 1 and 2 represent stress and strain values before and after, respectively, the strain-rate jump in the test. The strain-rate sensitivities that were calculated from this test are 0.008, 0.006, and 0.008 respectively with the jumps progressing from the lowest to the highest strain-rate. Thus, the DP 1180 used in this research is not considered to be overly strain-rate sensitive in this range of strain-rates. Consequently, the adjustable process parameters such as the crosshead velocity and the carriage speed influencing the rate of deformation are not expected to appreciably influence the recorded load levels during CBT testing, from the material properties point of view.

The custom experimental apparatus for CBT has been recently designed and presented in [17]. For completeness, some of the key features are briefly summarized here. The machine consists of four subsystems: (1) the moving carriage, (2) the stationary roller assembly, (3) the base, and (4) the data-acquisition and control hardware and software. The diameter of the rollers is D = 25.4 mm, imparting a nominal strain of 3.8% per roller engagement if a sheet of 1 mm wraps around it. The axes of the two lower rollers are L = 54 mm apart. The top roller is adjustable in the vertical direction, so that the bending depth, δ, can be varied (Fig. 1). The sensors in the apparatus consist of two donut-style Futek load-cells, one tension (LCF 450, capacity of 22.24 kN) and the other compression (LTH 500, capacity of 22.24 kN). The tension load-cell is attached to the actuator and the compression one to the carriage. The hydraulic actuator has a Balluff Micropulse BTL7-A501-M0305-Z-S32 position sensor with a resolution of 5 μm. Finally, the limit switches are positioned at the end of the stroke, signaling the reversion of the moving carriage direction. One of these limit switches is attached to the moving crosshead of the hydraulic actuator, and thus enables the progressive growth of each stroke, as the specimen elongates during CBT. The other one is attached to the roller assembly.

While the studies related to CBT available in the literature relied on universal testing machines equipped with a set of traversing rollers [18,19], the apparatus used in the present study has stationary rollers mounted on the machine base, while the specimen and its axial loading

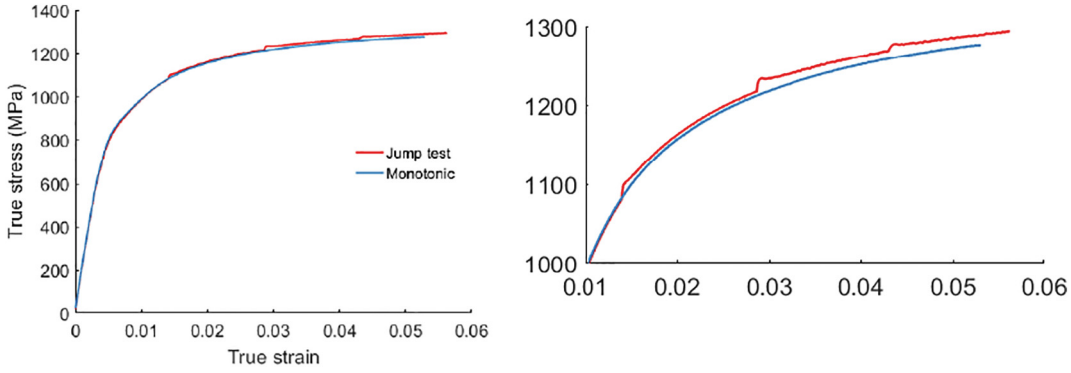

Fig. 3. Monotonic true stress-true strain curve for simple tension under 0.001/s strain rate along with a true stress-true strain curve with jumps in strain rate from 0.0001 to 0.001, from 0.001 to 0.005, and from 0.005 to 0.01/s for DP 1180 along TD.

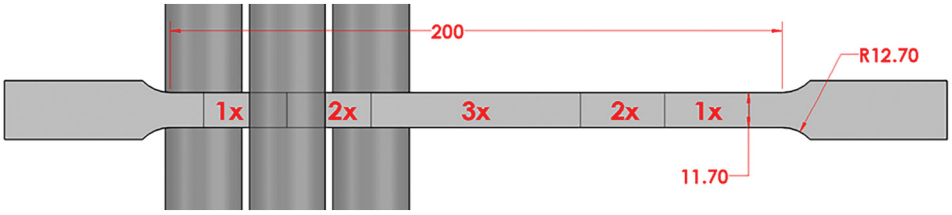

Fig. 4. Initial CBT specimen with dimensions in millimeters. The deformation regions (1×, 2×, and 3×) are indicated.

system is reciprocating. The nut of the ball-screw is attached to the carriage, so that the latter can reciprocate during the CBT experiments. The maximum practical carriage velocity is 66 mm/s, which is used in the present study. The advantage of our setup is in the fixed rollers, i.e., direct observation of the material flowing through the rollers, which enables the use of Digital Image Correlation (DIC) to study the strain accumulation per cycle, in real time. The DIC measurements will be reported in future works. Moreover, our apparatus is capable of processing sheets in addition to the strips which are studied here.

Fig. 4 shows a schematic of the CBT specimen with different deformation regions identified. These correspond to how many bending cycles the material in the region undergoes with each CBT cycle. A CBT cycle is defined as the rollers traversing the entire gauge length and then back again. Near the grips, the material only experiences one bending-unbending per cycle (1×), while the material in the center of the specimen is bent and unbent three times (3×) through the three rollers used in the CBT process. The gauge length of our CBT specimens is appropriately chosen to be 200 mm. Basically, the length of the gauge section was increased from the standard ASTM E8 tensile specimen so the rollers never exit it while producing the 1×, 2×, and 3× deformation regions. The CBT specimens were machined from the 1.04 mm thick DP 1180 sheet along RD, 45° and TD of the sheet material.

3. Results

Figs. 5 and 6 show the force vs. displacement curves recorded during CBT along RD, 45°, and TD for varying cross head velocity and for varying normalized bending depth with sheet thickness (δ/t), respectively. The crosshead velocity was varied from 0.6 mm/s to 2 mm/s, while the velocity of the carriage (i.e. roller-specimen relative velocity) was kept constant at 66 mm/s. The bending depth values are normalized to remove dependence of the results on the sheet thickness and ranged from 2 to 4.25. Also included in Fig. 6 are the ST curves along the three testing directions. The ST curves are recorded on identical specimens to those used in CBT. In fact, given that the ST specimens experience uniform elongation throughout their uniform section, while the CBT specimens receive the full number of CBT cycles only in the 3× region (see Fig. 4), the comparisons of ST and CBT in Fig. 6 is biased against the CBT results. As is evident from the comparison between the ST and CBT results, the axial force necessary to sustain the CBT process is significantly lower than the one needed to cause plastic flow in ST. More importantly, the ETF in CBT is significantly enhanced over that in ST. While the ST curves show typical work-hardening with a decreasing slope [32], the CBT curves exhibit a quasi-periodic pattern of spikes, which will be explained later.

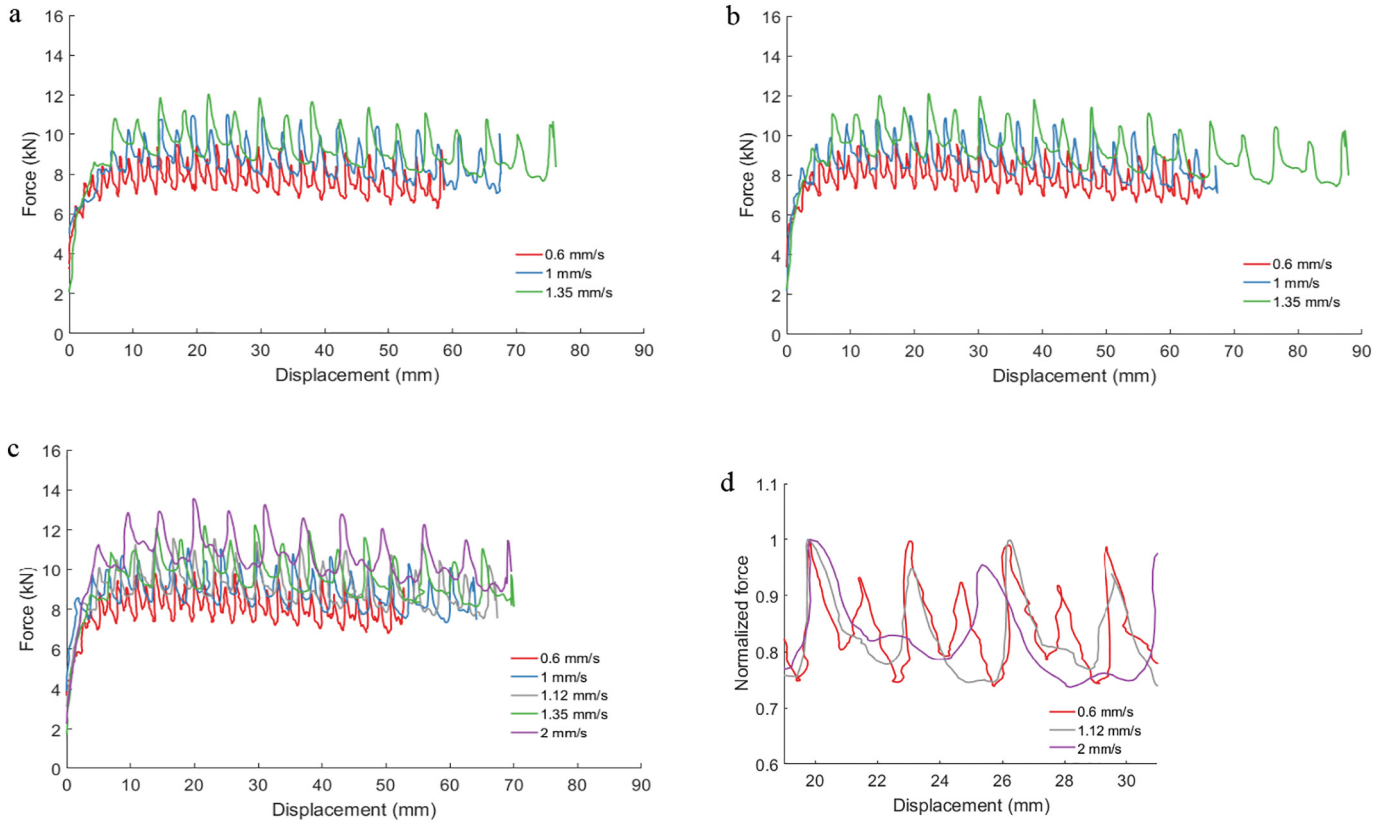

Fig. 5. Force-displacement curves for CBT tests along (a) RD, (b) 45°, and (c) TD under a normalized bending depth of 3.5 and varying crosshead velocities as indicated in the legends. (d) Inset showing the evolution of force normalized by the corresponding peak value for the selected crosshead velocities from (c).

With lowering crosshead velocity for a fixed δ/t value of 3.5 (Fig. 5), the measured force decreases in magnitude, meaning that more of the deformation is caused by bending than tension. With increasing crosshead velocities up to a certain level, even though there is more uniaxial tension deformation in the sheet causing higher forces, more displacement before fracture can be achieved. Further increase in the crosshead velocity (≥2) would reduce displacement before fracture. The area of contact between the rollers and the sheet reduces with an increase of crosshead velocity. This can be appreciated from Fig. 5d, which shows the variation of the period with the crosshead velocity for a constant bending depth. Since plastic deformation occurs only in the region underneath the rollers, the amount of the sheet exposed to uniaxial tension increases with crosshead velocity. As a result, the load increases. When the rollers momentarily stop and the test condition is similar to ST, the peaks are observed. The peak levels are also a consequence of the given test parameters. If the test is to continue under ST (without bending), the peak load would reach the same level corresponding to the load at yield in ST for every test. From the discrete tests carried out here, the optimal crosshead velocity of 1.35 mm/s is observed. The actual values of force amplitudes are not constant with varying crosshead velocities for the constant bending depth, as shown in Fig. 6a–c. However, the normalized amplitudes do not vary significantly. On the other hand, the periods do vary (Fig. 5d). It is interesting to point out that as the deceleration and acceleration time and distance are constant for these tests (since the rollers move independently on the crosshead velocity), increasing the crosshead velocity means that the strain rate while the rollers are accelerating/decelerating, i.e., when the CBT tends towards the ST test, is also increasing. This is because the sheet undergoing CBT is pulled faster over the given distance when the crosshead velocity is higher.

The bending depth, determines the extent of specimen wrapping around the rollers and, consequently, the amount of bending strain. This parameter has the effect of lowering the required force to deform the specimen for a given crosshead velocity, since the plastically deforming area of contact between the rollers and the sheet increases with the bending depth. Results in Fig. 6 are for the velocity of 1.35 mm/s. It is observed that the period of force is nearly constant, while the amplitude in force scales with the bending depth for the constant crosshead velocity (see Fig. 6d).

Fig. 7 summarizes the effect of process parameters on ETF during CBT testing for DP 1180. The ETF in CBT normalized by ETF in ST is shown for all three directions studied. As is evident, an optimal bending depth is around 3.5 for most cases, where the material is not under- or over-bent, and thus, more displacement before fracture (i.e., a higher ETF) is possible. If under-bent, the material is subjected to primarily uniaxial tension and thus fracture occurs at a lower displacement. If over-bent, additional bending strains are induced causing lower displacement values. Moreover, the effect of friction is likely more significant when the wrapping around the rollers increases. Observations in terms of the effect of bending depth and crosshead velocity on ETF based on the discrete tests performed here are regarded as close to optimal. A more in depth optimization study likely involving a combination of experiments and simulations should be carried out to arrive at true optimal values for these parameters maximizing ETF.

Fig. 8 shows the peak force occurring during the CBT tests as a function of normalized bend depth and crosshead velocity along the three studied directions. Note also that the plateau force, where most of the deformation accumulates, is well below the peak force. The drop in the force is approximately linear with increasing bend depth and

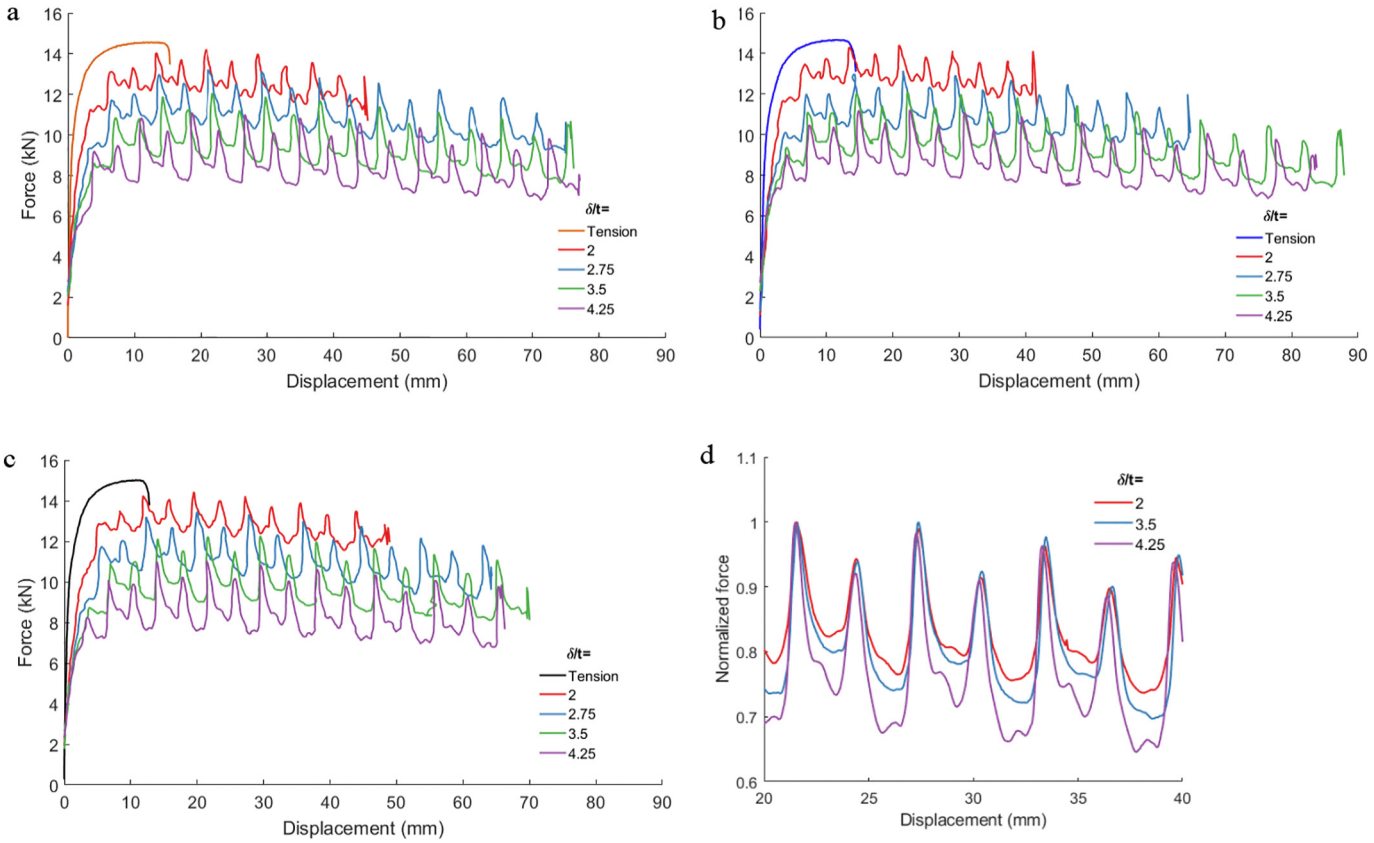

Fig. 6. Force-displacement curves for simple tension and CBT tests along (a) RD, (b) 45°, and (c) TD for a crosshead velocity of 1.35 mm/s and varying normalized bending depths as indicated in the legends. (d) Insert showing the evolution of force normalized by the corresponding peak value and shifted horizontally to a common point for the selected normalized bending depths from (a).

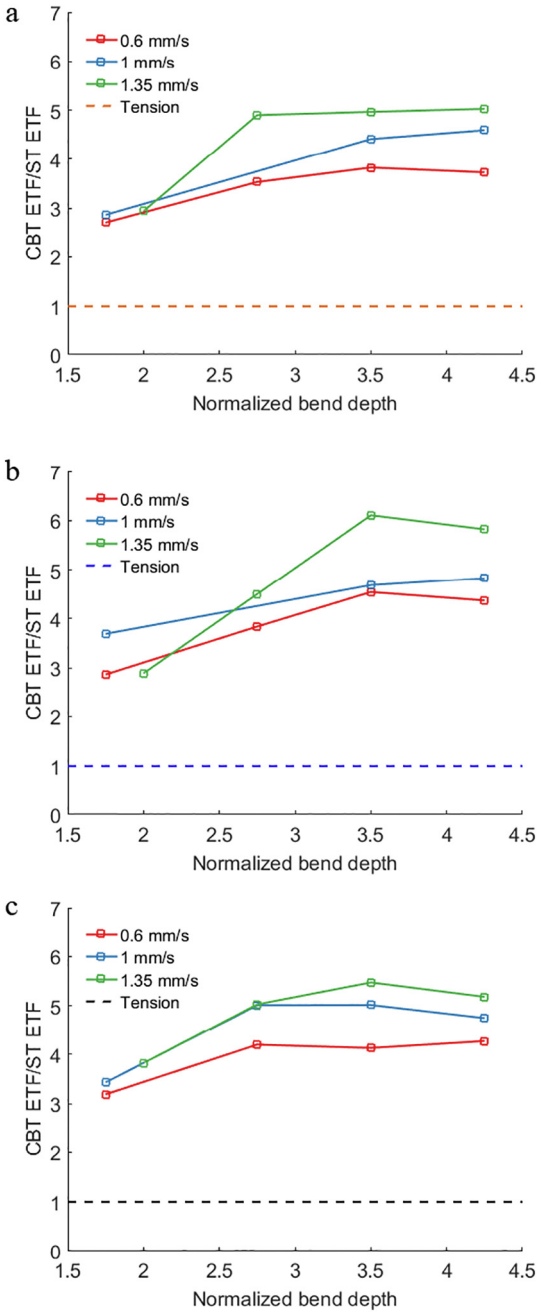

Fig. 7. Elongation-to-fracture (ETF) in CBT normalized by ETF in simple tension (ST) along (a) RD, (b) 45°, and (c) TD. The unity horizontal line which represents ST is also shown as a reference.

increases with the velocity. The maximum force recorded in tension at UTS is greater than any force recorded in CBT. Moreover, these results reveal that the plastic flow occurs mainly during the bending-unbending cycles since the axial force is even lower than the initial yield limit of the material for most of the testing conditions.

In summary, the CBT loading mode inhibits the localization of deformation and the appearance of necking. Hence the deformation can proceed to large strains, allowing the ductility to be depleted uniformly along the specimen. Eventually though, the allowable deformation in the material is achieved, at which time the material ruptures and the test terminates.

Fig. 9a shows photographs of specimens failed in CBT under a normalized bending depth of 3.5 and a crosshead velocity of 1.12 mm/s after 10.5 cycles (top) and in ST (middle) along TD. An undeformed specimen (bottom) is also included as a reference to assess the ETF in CBT vs. ST. The effect of CBT on ETF is considerable. Additionally, Fig. 9b shows a photograph of specimens processed by CBT under a normalized bending depth of 3.5 and a crosshead velocity of 1.35 mm/s to several values of CBT cycles along RD. The stress state in the specimens after CBT is such that it causes the specimens to permanently bend, which will be explained later. Also, the orientation of the fracture has changed, from the customary localized neck along the plane strain direction (54°, for an isotropic material) in the ST specimen, to perpendicular to the principal stress in the CBT one.

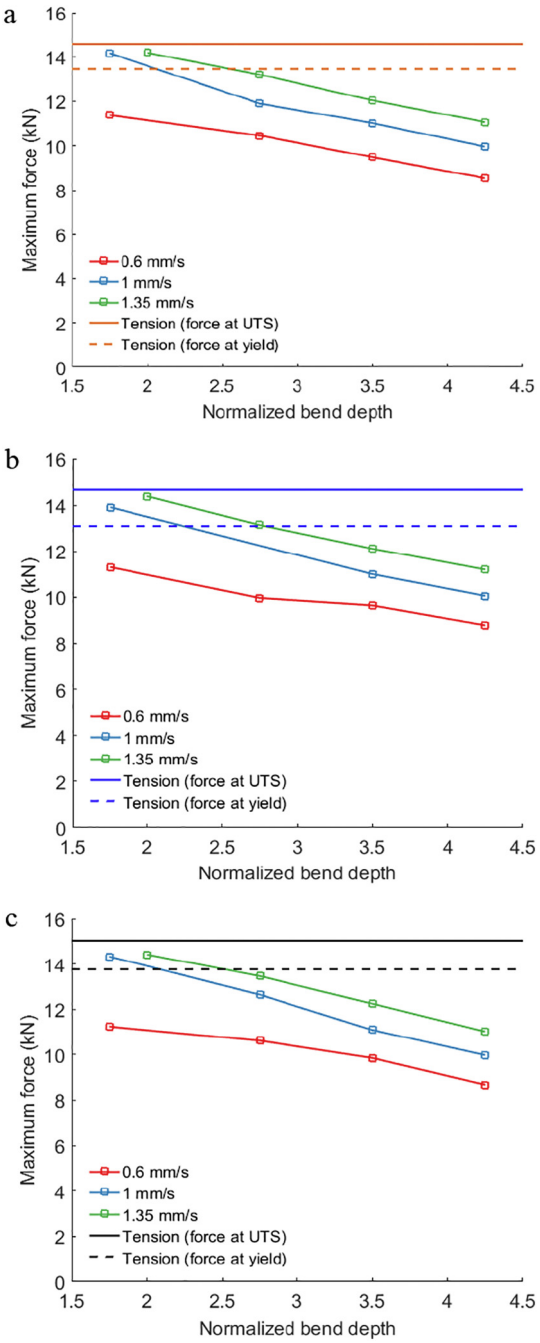

Fig. 8. Peak force occurring during CBT tests as a function of normalized bend depth and crosshead velocity along (a) RD, (b) 45°, and (c) TD. Horizontal lines which represent the UTS and yield force values in ST are also shown as references.

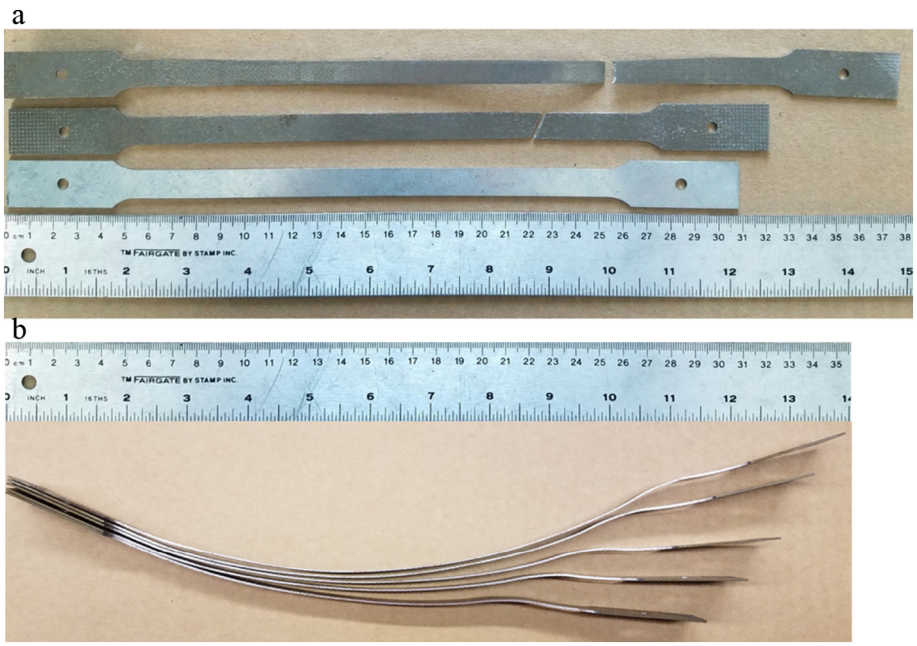

Fig. 9. (a) Comparison between failed specimens in CBT under a normalized bending depth of 3.5 and a crosshead velocity of 1.12 mm/s after 10.5 cycles (top) and ST (middle) along TD. An undeformed specimen (bottom) is included as a reference to assess the ETF in CBT vs. ST. (b) A photograph showing the shape and elongation of specimens after CBT processing under a normalized bending depth of 3.5 and a crosshead velocity of 1.35 mm/s as a function of CBT cycles along RD (2, 4, 6, 8, and 10 from bottom to top).

4. Discussion

Results in terms of the effect of CBT process parameters, namely the bending depth and crosshead velocity, demonstrate the remarkable effect of CBT on the ETF and the axial force level. The results are sensitive to both the crosshead velocity and the normalized bending depth. For the lowest value of the bending depths, the strip does not wrap well around the rollers, and as a result, the added bending strain per CBT stroke is small. Therefore, the strip is exposed to more ST. Increasing the bending depth improves the wrapping and thus increases the amount of bending strain per stroke. However, excessive bending can cause the strip to fail sooner. In summary, increasing the normalized bending depth and increasing the crosshead velocity increases the ETF, until a peak enhancement is reached. Furthermore, increasing the crosshead velocities and lowering the normalized bending depth increases the force levels during CBT. Under a normalized bending depth of 3.5 and crosshead velocity of 1.35 mm/s, ETF of DP 1180 improves over five times compared to ST for every tested direction.

To better understand the kinematics and the evolution strain fields during CBT, the process is simulated using finite element method. Simulations of the CBT process are numerically challenging for the standard FE solver in Abaqus due to a relatively complex kinematics and very large elongations, especially for the process parameters facilitating the greatest ETF. The process is successfully simulated under a normalized

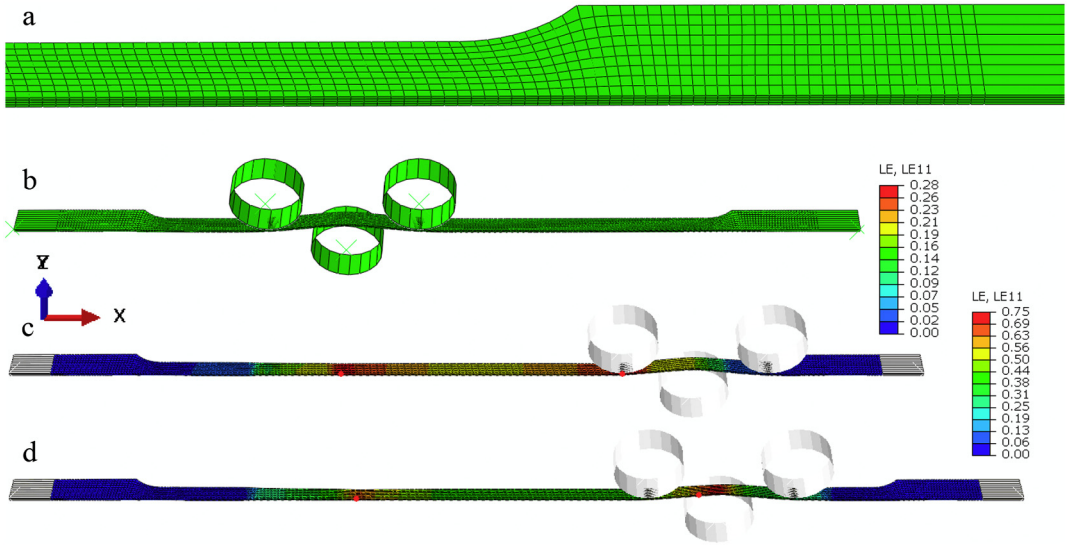

Fig. 10. Finite element simulation setup and axial strain contours developing during the CBT process simulated in Abaqus under a normalized bending depth of 3.5 and crosshead velocity of 1.12 mm/s: (a) initial mesh of the ½ FE model consisting of 9831 C3D8R elements, and three instances during CBT simulation: (b) upon rollers first engagement (before pulling and reciprocating), (c) in middle of the process (after 5.5 CBT cycles), and (d) at the end of the process (after 10.5 CBT cycles). The evolution of the 3× deformation regions is indicated in (c) and (d) by red dots. As the frame shows, the view is tilted for 45° about X (TD). (For interpretation of the references to color in this figure legend, the reader is referred to the web version of this article.)

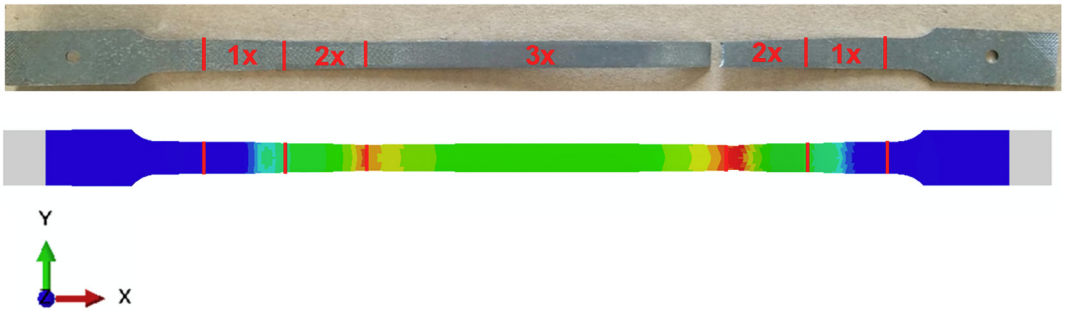

Fig. 11. Comparison between experimentally deformed specimen from Fig. 9a and FE simulation from Fig. 10d. The axial strain contours show the strain localization regions. The color legend is the same as in Fig. 10d. (For interpretation of the references to color in this figure legend, the reader is referred to the web version of this article.)

bending depth of 3.5 and a crosshead velocity of 1.12 mm/s, and these results are presented. Fig. 10 shows the simulation setup in Abaqus and axial strain contours developing during CBT in the strip. The velocity boundary conditions are directly applied to the sheet, while the rollers as objects of D = 25.4 mm induce the bending, consistent with the experiment. The roller velocity profile recorded during the experiment is applied in the simulation. The profile will be shown and explained shortly. The initial mesh of the ½ FE model consists of 9831 C3D8R (continuum three-dimensional eight nodal with reduced integration) elements. After performing a mesh-sensitivity study, we observed that further refinement of the mesh leaves the results unchanged. Adding more elements would only increase the computational time involved in the simulation. The simulations were carried out using the rate-independent plasticity theory of von Mises (also known as J_2) with a yield surface that can expand isotropically based on the given true stress-true strain curve for DP 1180 along TD. The J_2 plasticity model is available in Abaqus [33]. The ST curve was appropriately extrapolated to match the CBT load vs. displacement data. The axial strain along the specimen varies between the 1×, 2× and 3× regions, with the latter achieving the highest strain levels. Noticeably, axial strain concentrates at the boundary between 2× and 3× deformation regions, which is where failures in experiments are observed as well. We will refer to this region as the hot spot. Axial strain (LE11) is predicted to accumulate with CBT cycles from 0.039 in the first CBT cycle, over 0.085, 0.135, 0.185, 0.236, 0.288, 0.347, 0.405, 0.47, and 0.557 in subsequent cycles to 0.577 in the last cycle (10.5). These values were taken from the central region (in the middle of the 3× region) of the sample. The corresponding strain levels in the hot spots are 0.051, 0.098, 0.146, 0.2, 0.255, 0.31, 0.369, 0.434, 0.507, 0.614 and 0.704.

The width and thickness of the failed CBT specimen in Fig. 9a were measured using a micrometer for each deformation region (1×, 2×, and 3×). From multiple measurements, the average width is 11.19 mm, 10.29 mm, and 10.01 mm for 1×, 2×, and 3× deformation regions, respectively. The average thickness is 1.03, 0.871, and 0.827 for

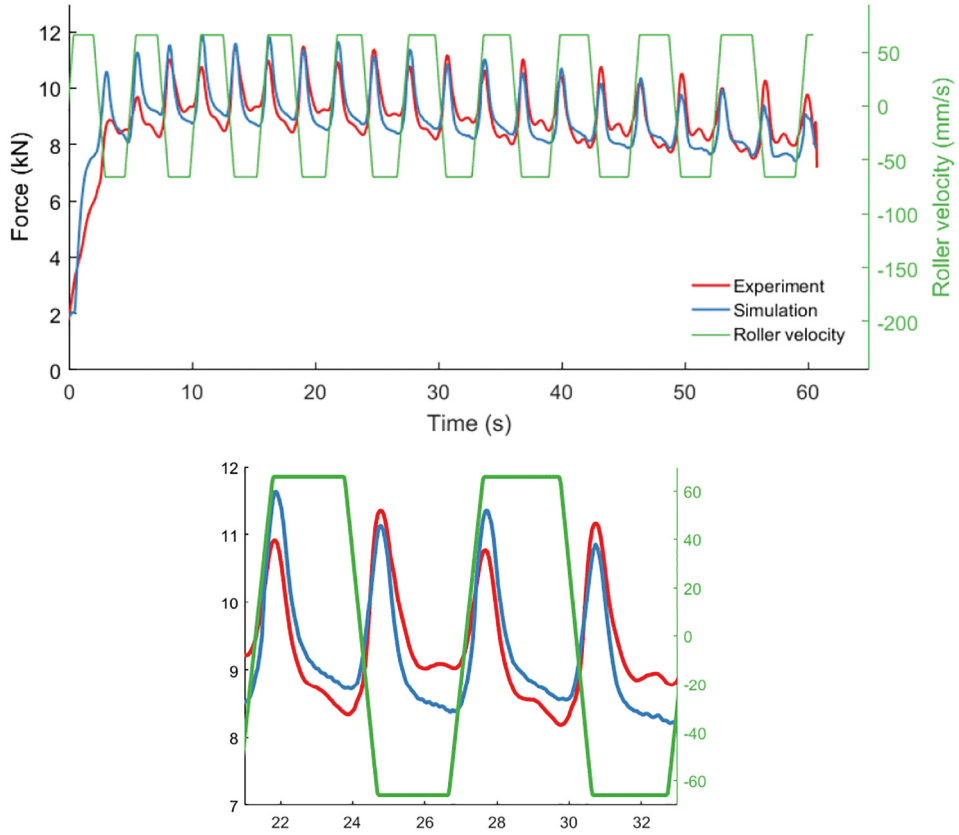

Fig. 12. Comparison between measured and simulated time evolution of force along with the roller velocity profile during CBT under a crosshead velocity of 1.12 mm/s and a normalized bending depth of 3.5 along the TD. The insert is a magnified snapshot highlighting the correlation between the force and velocity profiles during CBT.

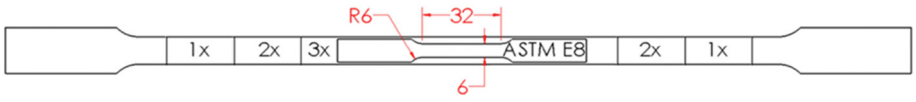

Fig. 13. CBT specimen after deformation along with the sub-size specimen for subsequent ST. The dimensions are in millimeters. The deformation regions (1×, 2×, and 3×) are indicated.

1×, 2×, and 3×, respectively. The measurements reveal that the regions indeed experience different levels of plastic strain. As a result, geometric discontinuities develop primarily at the locations where the deformation regions meet. The most severe stress/strain concentrations develop at the location where 2× and 3× deformation regions meet. We again have observed that most of the tested samples fail around that location. Fig. 11 shows the comparison between the experimentally deformed specimen from Fig. 9a and the FE simulation from Fig. 10d. As is evident, the predicted localization region in axial strain is the location of fracture.

Fig. 9a shows that the fracture of the CBT specimen is perpendicular to the loading direction, with little to no signs of necking. This corroborates the earlier statement that CBT suppresses the necking instability. On the other hand, the ST specimen failed in the typical localized neck fashion, with the neck inclined to the loading direction at a ~54° angle.

It is worth mentioning that a specimen undergoing CBT, depending on its geometry, can experience from plane strain to simple tension stress/strain state. Without bending, the narrow specimen geometry like the strip used in the present work is in simple tension. However, if the strip specimen is replaced with a much wider specimen like a sheet, the stress/strain state in the sheet can approach plane strain tension. Depending on the sheet width relative to the roller radius, bending of a sheet metal is generally expected to be plane strain, at least away from its free edges.

To provide better insights into the kinematics of the process and the shape of the curves shown in Figs. 5 and 6, we superimpose the force-time and roller velocity-time data in a single plot. Fig. 12 shows such a plot combining the measured and simulated data. The simulation is regarded to capture the measured data very well, considering the simple J_2 plasticity constitutive description of the material. The predictions could be improved by involving more accurate material models such as those based on crystal plasticity theory incorporating the kinematic hardening effects [34].

At the beginning of each stroke, the carriage accelerates linearly and then attains a constant velocity, which is maintained for the majority of the stroke (Fig. 12). It then decelerates linearly until it stops; this profile is repeated during every stroke. The force spikes occur during the deceleration and acceleration phases. Essentially, the bending is momentarily paused, and the specimen approaches the tensile condition. Hence the force raises, to meet the force required for plastic flow under ST. However, soon enough the carriage starts moving in the opposite direction, resuming the CBT loading condition, which manifests itself in the force drop. The height of the spikes scales with the amount of bending (see Fig. 6d). Between the peaks there is roughly a plateau in the force as the deformation is near steady state. Note that there is a slight difference between the force values for every other plateau. This is caused by the material either moving towards (lower plateau force) or away from (higher plateau force) the measuring load cell. Furthermore, Fig. 12 shows that as CBT progresses, the load-bearing capacity of the specimen is reduced, despite the additional work-hardening that is expected to occur. This must be attributed to the contraction of the width and thickness, as the specimen elongates.

5. Strength and residual ductility after CBT processing

Fig. 9b shows the shape of interrupted CBT strips treated to a certain number of CBT cycles (we remind that a CBT cycle is defined as the rollers traversing the entire gauge length and then back again). After the specified number of cycles was achieved, the specimen was removed from the CBT machine. The specimens were found to have an increasing amount of residual curvature with the cycles when removed from the CBT machine (see Fig. 9b), which indicated a non-symmetric process induced stress profile. The curved CBT specimens were fixtured to machine sub-size tensile specimens using wire-EDM for subsequent ST, as schematically shown in Fig. 13. The sub-size specimens were machined from the 3× deformation region. The bending stress in the specimens is relatively small, as could be verified easily by straightening the curved specimens by hand before installing them in the tensile testing machine. If the specimens are released before ST testing, they return to similar curvatures before straightening.

The CBT experiments were used to process the material and probe its response past the limit of uniform deformation in ST. The motivation of such an experiment is four-fold: (1) increase strength of the material,

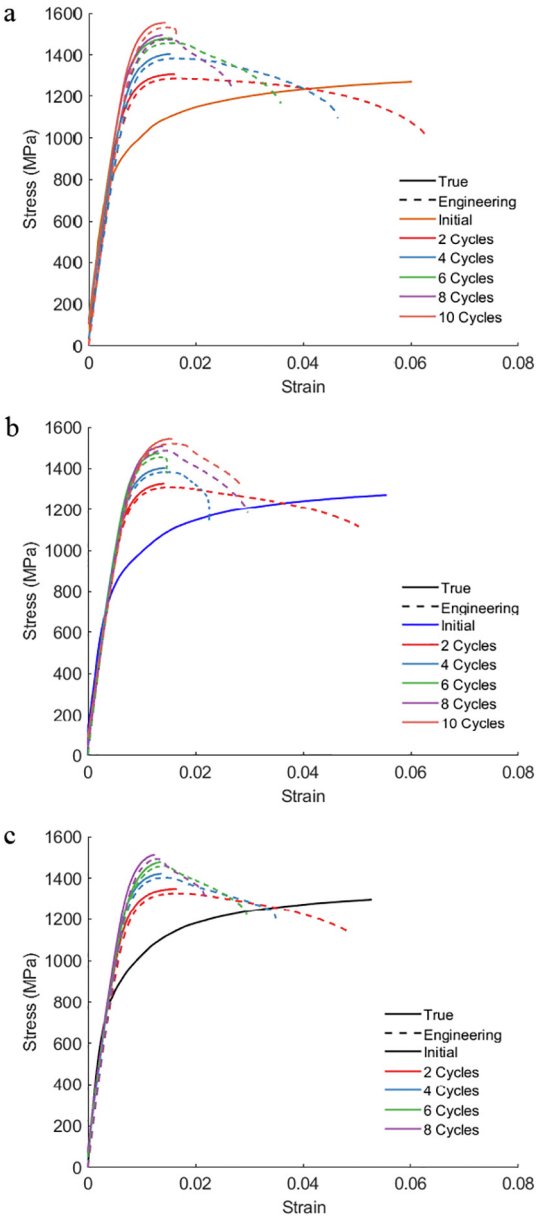

Fig. 14. Engineering stress-strain and true stress-strain curves based on monotonic ST of sub-size specimens machined from the interrupted CBT test specimens processed to the number of cycles as indicated in the legends along: (a) RD, (b) 45°, and (c) TD.

Table 1
Material parameters obtained from simple tension tests. Dash symbol in the table indicates either not a reliable measurement or not measured.

	RD				45°				TD			
# of CBT cycles	E (GPa)	YS (MPa)	UTS (MPa)	R-ratio	E (GPa)	YS (MPa)	UTS (MPa)	R-ratio	E (GPa)	YS (MPa)	UTS (MPa)	R-ratio
0 (initial)	203	842	1187	0.95	205	850	1184	0.97	214	849	1222	0.84
2	–	1198	1285	1.14	208	1206	1311	1.17	208	1207	1328	1.23
4	–	1311	1386	1.10	213	1285	1386	1.23	207	1315	1405	1.10
6	204	1355	1459	–	207	1370	1456	–	210	1365	1460	–
8	204	1357	1470	–	193	1407	1489	–	208	1412	1495	–
10	197	1454	1534	–	178	1417	1522	–	–	–	–	–

(2) evaluate residual ductility for the increased strength, (3) change the material microstructure for enhancing material properties upon an appropriate heat treatment, and (4) extrapolate the stress-strain behavior to larger strain levels than achieved during ST.

Even though some bending stress left from the CBT pre-straining is present in every specimen, we tested the sub-size specimens in ST, thus superimposing the tensile stress and strain state over the residual stress. Engineering stress-strain and true stress-strain curves measured along RD, 45°, and TD are presented in Fig. 14. The strength of the material treated by CBT increases over the as-received material and with the CBT cycles, while the residual ETF reduces. Table 1 presents Young's modulus (E), yield strength (YS), ultimate tensile strength (UTS), and R-ratio obtained from ST tests for all specimens. The R-ratio is defined as the ratio between the in-plane plastic strain in the direction perpendicular to the loading direction and the plastic strain in the through-thickness normal direction. The elastic slope was taken from the curves between 200 MPa and 900 MPa because stresses below 200 MPa were slightly nonlinear due to sample straightening. The elastic slope of the material increases but after 10 CBT cycles it drops, likely because of significant damage is accumulated in the material. Note that 10 cycles were not achievable in the TD samples without failure in the CBT tests. Interestingly, crystallographic texture and microstructure in the material evolve such that the R-ratio improves, i.e., less thickness strain, upon CBT. The R-ratio strongly depends on texture in the material [35]. Texture of body-centered cubic materials deformed in tension evolves to form a ⟨011⟩ fiber texture, where these planes align with the pulling direction [36]. The ⟨011⟩ fiber texture exhibits a high value of R-ratio [36,37]. Since the CBT process evolves texture in the material similar to tension [17], it can be expected that the R-ratio improves. However, since the evolution of texture and microstructure in DP 1180 is very complex due to multiple phases of different deformation characteristics, future research is necessary to reveal the origin of improved R-ratio in CBT. R-values for the higher CBT cycle tests are not reported since little ductility is achieved after yielding to obtain reliable data. Subsequent research will attempt to restore the ductility of the material while preserving the R-ratio by appropriate heat treatment. Furthermore, future research will evaluate if the post CBT material testing could provide a method for determining the stress-strain behavior of a material beyond what is able to be achieved with a uniaxial tension test.

In closing, we point out that reciprocating rollers or a wavy contour over which the sheet traverses could be incorporated into drawing processes, either in the binder area or in the forming cavity, in order to take advantage of the enhanced elongation observed in CBT processing.

6. Conclusions

This work utilized a recently built experimental setup for CBT of thin strips and sheets to evaluate ETF enhancements of DP 1180 steel under such CBT conditions. In particular, the effect of process parameters such as crosshead velocity and bending depth on the ETF and the reduction of axial force are presented for the material. The force vs. displacement response is found to be a strong function of both of these parameters. From the detailed analysis of the data, the optimal parameters for enhancing ductility of DP 1180 under CBT are approximately 1.35 mm/s for crosshead velocity and 3.5 for normalized bending depth. Under these conditions, the material elongates over five times more than in ST. Such improvements are achieved because the CBT process incrementally elongates the entire gauge length of the specimen as much as possible before fracture occurs by preventing localization of deformation and the necking instability. Remarkably, these improvements obtained for DP 1180 are far beyond what has been achieved for AA6022-T4 using the same equipment and methodology, and other materials in the literature [18]. The FE simulation of the process was used to better reveal the kinematics of the process and to predict stress and strain fields developing during the process. The predicted location of the localization is where 2× and 3× deformation regions meet, which agrees well with the failure location for many tested specimens in CBT. This work demonstrated the improvements in sheet metal formability that can be obtained using the CBT operation for DP 1180 steel. However, it also provided a promising means to evaluate material flow prior to fracture for other AHSS and many other materials when subjected to CBT processing. The work further showed that taking advantage of CBT processing the material can significantly increase its strength. Here, sub-size tensile specimens extracted from the CBT treated strips of DP 1180 were tested in ST and found to exhibit a higher yield stress and decreased elongation relative to the ST response of the as-received material. The strength of the material increased with the number of CBT cycles.

CRediT authorship contribution statement

Camille M. Poulin: Investigation, Methodology, Validation, Formal analysis. **Yannis P. Korkolis:** Conceptualization, Writing - review & editing, Supervision, Funding acquisition. **Brad L. Kinsey:** Conceptualization, Supervision, Funding acquisition. **Marko Knezevic:** Conceptualization, Methodology, Writing - original draft, Writing - review & editing, Supervision, Project administration.

Acknowledgements

CP and MK are grateful for financial support to the U.S. National Science Foundation under the CAREER grant no. CMMI-1650641. The custom CBT equipment was designed and built under grant no. CMMI-1301081.

Data availability

The raw/processed data required to reproduce these findings cannot be shared at this time due to technical or time limitations.

References

[1] M. Calcagnotto, D. Ponge, D. Raabe, Microstructure control during fabrication of ultrafine grained dual-phase steel: characterization and effect of intercritical annealing parameters, ISIJ Int. 52 (2012) 874–883.
[2] W. Woo, V.T. Em, E.Y. Kim, S.H. Han, Y.S. Han, S.H. Choi, Stress–strain relationship between ferrite and martensite in a dual-phase steel studied by in situ neutron diffraction and crystal plasticity theories, Acta Mater. 60 (2012) 6972–6981.

[3] H. Gong, S. Wang, P. Knysh, Y.P. Korkolis, Experimental investigation of the mechanical response of laser-welded dissimilar blanks from advanced- and ultra-high-strength steels, Mater. Des. 90 (2016) 1115–1123.
[4] B. Ma, Z.G. Liu, Z. Jiang, X. Wu, K. Diao, M. Wan, Prediction of forming limit in DP590 steel sheet forming: an extended fracture criterion, Mater. Des. 96 (2016) 401–408.
[5] A. Ghaei, D.E. Green, A. Aryanpour, Springback simulation of advanced high strength steels considering nonlinear elastic unloading–reloading behavior, Mater. Des. 88 (2015) 461–470.
[6] M. Calcagnotto, Y. Adachi, D. Ponge, D. Raabe, Deformation and fracture mechanisms in fine- and ultrafine-grained ferrite/martensite dual-phase steels and the effect of aging, Acta Mater. 59 (2011) 658–670.
[7] M. Bhargava, S. Chakrabarty, V.K. Barnwal, A. Tewari, S.K. Mishra, Effect of microstructure evolution during plastic deformation on the formability of Transformation Induced Plasticity and Quenched & Partitioned AHSS, Mater. Des. 152 (2018) 65–77.
[8] C.C. Tasan, J.P.M. Hoefnagels, M. Diehl, D. Yan, F. Roters, D. Raabe, Strain localization and damage in dual phase steels investigated by coupled in-situ deformation experiments and crystal plasticity simulations, Int. J. Plast. 63 (2014) 198–210.
[9] M. Kapp, T. Hebesberger, O. Kolednik, A micro-level strain analysis of a high-strength dual-phase steel, Int. J. Mater. Res. 102 (2011) 687–691.
[10] R.H. Wagoner, J.H. Kim, J.H. Sung, Formability of advanced high strength steels, Int. J. Mater. Form. 2 (2009) 359.
[11] H.K.D.H. Bhadeshia, TRIP-assisted steels? ISIJ Int. 42 (2002) 1059–1060.
[12] M. Shi, S. Gelisse, Issues on the AHSS forming limit determination, Proceedings of the IDDRG International Conference, Porto, Portugal 2006, pp. 19–21.
[13] C. Nikhare, P. Hodgson, M. Weiss, Necking and fracture of advanced high strength steels, Mater. Sci. Eng. A 528 (2011) 3010–3013.
[14] N. Saeidi, F. Ashrafizadeh, B. Niroumand, F. Barlat, EBSD study of micromechanisms involved in high deformation ability of DP steels, Mater. Des. 87 (2015) 130–137.
[15] X. Xue, J. Liao, G. Vincze, J. Sousa, F. Barlat, J. Gracio, Modelling and sensitivity analysis of twist springback in deep drawing of dual-phase steel, Mater. Des. 90 (2016) 204–217.
[16] O. Bouaziz, H. Zurob, M. Huang, Driving force and logic of development of advanced high strength steels for automotive applications, Steel Res. Int. 84 (2013) 937–947.
[17] M. Zecevic, T. Roemer, M. Knezevic, Y. Korkolis, B. Kinsey, Residual ductility and microstructural evolution in continuous-bending-under-tension of AA-6022-T4, Materials. 9 (2016) 130.
[18] W.C. Emmens, A.H. van den Boogaard, Incremental forming by continuous bending under tension—an experimental investigation, J. Mater. Process. Technol. 209 (2009) 5456–5463.
[19] J. Benedyk, N. Parikh, D. Stawarz, A method for increasing elongation values for ferrous and nonferrous sheet metals (Ferrous and nonferrous sheet metals neck formation prevention for increasing elongation in tensile tests, using continuous plastic bending method), J. Mater. 6 (1971) 16–29.
[20] H. Swift, Plastic bending under tension, Engineering 166 (1948) 333–359.
[21] H. Nine, Drawbead forces in sheet metal forming, Mechanics of Sheet Metal Forming, Springer, Boston, MA 1978, pp. 179–211.
[22] O. Music, J. Allwood, K. Kawai, A review of the mechanics of metal spinning, J. Mater. Process. Technol. 210 (2010) 3–23.
[23] E. Quigley, J. Monaghan, Metal forming: an analysis of spinning processes, J. Mater. Process. Technol. 103 (2000) 114–119.
[24] L. Wang, H. Long, Investigation of material deformation in multi-pass conventional metal spinning, Mater. Des. 32 (2011) 2891–2899.
[25] W.C. Emmens, G. Sebastiani, A.H. van den Boogaard, The technology of incremental sheet forming—a brief review of the history, J. Mater. Process. Technol. 210 (2010) 981–997.
[26] J.M. Allwood, D.R. Shouler, A.E. Tekkaya, The increased forming limits of incremental sheet forming processes, Key Eng. Mater. 344 (2007) 621–628.
[27] Y. Huang, J. Cao, K. Smith, B. Woody, J. Ziegert, M. Li, Experimental and numerical investigation of forming limits in incremental forming of a conical cup, Transactions of the North American Manufacturing Research Institution of SME, 2008.
[28] W.C. Emmens, A.H. van den Boogaard, An overview of stabilizing deformation mechanisms in incremental sheet forming, J. Mater. Process. Technol. 209 (2009) 3688–3695.
[29] https://www.ussteel.com/products-solutions/products/dual-phase-1180 2018.
[30] N. Deng, Y.P. Korkolis, Elastic anisotropy of dual-phase steels with varying martensite content, Int. J. Solids Struct. 141-142 (2018) 264–278.
[31] W.F. Hosford, R.M. Caddell, Metal Forming: Mechanics and Metallurgy, Cambridge University Press, New York, USA, 2011.
[32] M. Knezevic, I.J. Beyerlein, Multiscale modeling of microstructure-property relationships of polycrystalline metals during thermo-mechanical deformation, Adv. Eng. Mater. 20 (2018), 1700956. .
[33] ABAQUS Version 6. , Dassault Systèmes, Providence, RI, USA, 2017.
[34] M. Zecevic, Y.P. Korkolis, T. Kuwabara, M. Knezevic, Dual-phase steel sheets under cyclic tension–compression to large strains: experiments and crystal plasticity modeling, J. Mech. Phys. Solids. 96 (2016) 65–87.
[35] M. Zecevic, M. Knezevic, Latent hardening within the elasto-plastic self-consistent polycrystal homogenization to enable the prediction of anisotropy of AA6022-T4 sheets, Int. J. Plast. 105 (2018) 141–163.
[36] U.F. Kocks, C.N. Tomé, H.-R. Wenk, Texture and Anisotropy, Cambridge University Press, Cambridge, UK, 1998.
[37] M. Knezevic, S.R. Kalidindi, R.K. Mishra, Delineation of first-order closures for plastic properties requiring explicit consideration of strain hardening and crystallographic texture evolution, Int. J. Plast. 24 (2008) 327–342.